Capacitance-voltage characteristics of a 4,4′-bis[(N-carbazole)styryl]biphenyl based organic light-emitting diode: Implications for characteristic times and their distribution

Le Zhang,[1,2] Hajime Nakanotani,[1] and Chihaya Adachi[1,2,a]

[1]*Center for Organic Photonics and Electronics Research (OPERA), Kyushu University, 744 Motooka, Nishi, Fukuoka 819-0395, Japan*
[2]*International Institute for Carbon Neutral Energy Research (WPI-I2CNER), Kyushu University, 744 Motooka, Nishi, Fukuoka 819-0395, Japan*

The characteristic times and their distributions of a fluorescent 4,4′-bis[(N-carbazole)styryl]biphenyl-based organic light-emitting diode (OLED) were studied using impedance spectroscopy. The four defined characteristic times (transit time, recombination time, trapping time, and ac characteristic time) and their dc bias dependences were obtained from the frequency dependence of capacitance. The trapped carrier density distribution in the time domain was revealed from the voltage dependence of the OLED. The relative value of each characteristic time is suggested to play an important role in determining the profile of the frequency- and voltage-dependent capacitance of OLEDs. © 2013 AIP Publishing LLC. [http://dx.doi.org/10.1063/1.4819436]

Organic light-emitting diodes (OLEDs) have developed rapidly in the last few decades from academic studies to real applications.[1–3] The basic carrier processes for device operation are bipolar carrier injection, transportation, exciton formation, and radiative recombination, which have all been intensively studied, individually.[3,4] Among these processes, carrier transport mechanisms and dynamics of the generated excitons (both singlets and triplets) are of importance for further optimizing the device performance.[5–8] As one of the effective and convenient experimental approaches, impedance spectroscopy has been widely used to give a full description of the carrier behaviour in various organic electronic devices.[4,9–12]

With regard to the carrier transport process in OLEDs, it has been suggested that the decrease in capacitance below geometric capacitance and its subsequent increase in the lower frequency region of impedance spectroscopy was due to the redistribution of the injected carriers, which was theoretically analyzed by using the space-charge limited current (SCLC) theory with trapping effects and field dependent mobility.[13,14] In addition, both single and double carrier mobilities have been revealed from the frequency dependent susceptance measurement ($-\Delta B = -\omega(C - C_g)$, where ω is angular frequency and C_g is geometric capacitance), which exhibited good agreements with mobilities obtained using other methods.[15–17] On the other hand, the negative capacitance observed in the lower frequency region of impedance spectroscopy has been attributed to the radiative recombination process in OLEDs.[18–20] Although previous studies have shed much light on the carrier behaviour of OLEDs, they mainly focused on frequency dependence and related analysis rather than voltage dependence.[13–19] In addition, few comparative studies on the characteristic times have been performed, which, however, are of importance for a deep understanding about the device performance. Since the

capacitance-voltage relationship is directly related to the amount of space charge changes inside a device, i.e., $\Delta Q = C\Delta V$, it is expected that a different and more detailed picture of the carrier behaviour could be revealed.

In the present study, by using a highly fluorescent material 4,4′-bis[(N-carbazole)styryl]biphenyl (BSB-Cz),[21] the capacitance-voltage characteristics were studied with a focus on the space charge distribution, and characteristic times and their relationship. For the analysis of impedance spectroscopy, first of all, it is a quasi-steady-state measurement. The small ac signal generates additional carriers. The transport of those carriers is modified by the space charge field, which is formed by the dc bias.[9,10] In addition, there are several characteristic times defining the dynamic carrier behaviour, which are carrier transit time ($\tau_{tr} = L^2/\mu V_{dc}$, where L is the thickness of the active layer, μ is mobility, and V_{dc} is the applied dc voltage), trapping time ($\tau_{trap} = (\sigma\langle v_{th}\rangle N_t)^{-1}$, where σ is the trap capture cross section, $\langle v_{th}\rangle$ is the average thermal velocity and N_t is the overall number of trap states), recombination time (τ_r), and ac characteristic time ($\tau_{ac} = 1/f$, where f is the frequency). The relative values of these characteristic times and their dependencies on voltage have a great influence on the capacitance-voltage characteristics of a device. Among them, it was suggested that the trapping time (τ_{trap}) is not only voltage dependent but also exhibits a time distribution,[13,14] both of which can be well explored in the capacitance-voltage relationship.

The devices used here have a homo-junction triple-layer diode structure. A patterned indium tin oxide (ITO) substrate was used as a transparent anode after cleaning and UV/ozone treatment. Then, a hole injection layer of MoO_3 (5 wt. %) doped BSB-Cz layer with a thickness of 20 nm was evaporated on the ITO surface. Next, a neat BSB-Cz layer with a thickness of 200 nm was deposited. Subsequently, a 50 nm thick doped layer of Cs (10 wt. %) in BSB-Cz was deposited as an electron injection layer. Finally, an Ag electrode with a thickness of 100 nm was deposited as the cathode. During

a)Electronic mail: adachi@cstf.kyushu-u.ac.jp

the evaporation processes, the vacuum pressure was kept to about 10^{-4} Pa. The film thickness was monitored using a quartz crystal microbalance (QCM) and the evaporation rate was about 1.5 Å/s. All the devices were encapsulated in dry nitrogen atmosphere shortly after fabrication. Detailed descriptions of the fabrication and electrical characterization processes can be found in our previous paper.[21] The impedance spectroscopy was measured with a Solartron 1260 impedance/gain-phase analyzer at room temperature in the frequency region from 10 Hz to 1 MHz and under dc bias from -2 to 8 V. The amplitude of the ac signal was kept at 300 mV as a compromise between data stability and a linear response requirement. In fact, we found that the impedance spectroscopy was not affected much by ac amplitude up to 500 mV.

Figure 1 shows the current-voltage-luminance (J-V-L) and capacitance-voltage (C–V) characteristics of the BSB-Cz OLED. The C–V characteristics were measured at a frequency of 100 Hz. The inset of Fig. 1 shows the device structure. From Fig. 1, it can be seen that three curves corresponded to each other very well. The current density exhibited a power dependence on applied voltage (V_{dc}), i.e., $J \propto V_{dc}^6$, implying trap charge-limited current behaviour.[22] As the forward bias increased above 3 V, blue emission ($\lambda_{EL} = 470$ nm) was observed with a luminance of over 10^3 cd/m^2 and external quantum efficiency of over 0.5% at 10 V. The electroluminescent process of the OLED was also clearly revealed in its C–V characteristics.[11,20] Depending on the dc bias, capacitance can be written as three parts:

$$C = \frac{dQ}{dV} = \frac{dQ_m + dQ_{ac}^t - dQ_r}{dv_{ac}}. \quad (1)$$

Here, Q is the charge amount due to the perturbation ac signal v_{ac}. Q_m is the charge amount for the electrode charging process ($V_{dc} < 2$ V), i.e., $Q_m = C_g v_{ac}$ (C_g is the geometric capacitance, which was estimated to be about 445 pF for an electrode area of 4 mm^2, layer thickness of 270 nm and relative dielectric constant of 3.4 obtained from a single-layer device). Q_{ac}^t is the trapped charge amount (τ_{trap})

induced by the injected carriers ($V_{dc} > 2$ V). The positive value of this term indicates the redistribution of injected carriers with a finite transit time (τ_{tr}), which increases the capacitance in the lower frequency region.[13,14] Within the voltage region, no charge recombination or light emission was observed, implying that the space charges were mainly injected holes owing to their one order higher mobility than that of electrons.[21] Finally, at higher voltages ($V_{dc} > 3$ V), the recombination charge $Q_r(\tau_r)$ dominates. The recombination process consumes the injected carriers, resulting in a rapid decrease in capacitance, which can even become negative.[18–20] From the above, it can be seen that the individual electroluminescent processes in an OLED (bipolar injection, transport, trapping, and radiative recombination) can be well revealed and analyzed from the C–V characteristics.

The dependence of capacitance on frequency at various dc biases was shown in Fig. 2. At lower dc bias ($V_{dc} < 3$ V), the device behaved just like a dielectric layer with a capacitance of around 460 pF, corresponding well to the estimated value. As V_{dc} increased, a peak structure was observed in the lower frequency region, which is proposed to be closely related to the carrier behaviour inside the OLED. The increase in capacitance and its subsequent decrease to negative value are attributed to the redistribution of injected carriers and recombination processes, respectively.[13,14,18–20] In addition, it can been seen that the peak position and height varied with bias voltage, implying a competition between the carrier redistribution and recombination processes. In other words, the recombination processes, which dominated at higher dc bias, undermined the establishment of space charges. To better understand these processes, their characteristic times should be determined. If the underlying physics of those processes are considered, a simplified equation can be used to obtain both the trapping time (τ_{trap}) and relaxation time (τ_r)[14,19,23]

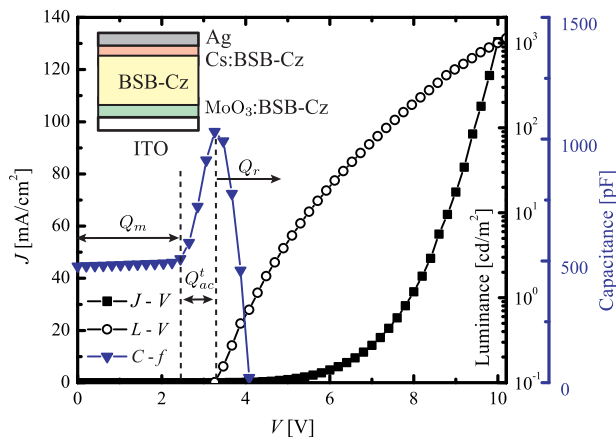$$C(\omega) = C_g + \frac{\chi_1 C_g}{1 + \omega^2 \tau_{trap}^2} - \frac{\chi_2 C_g}{1 + \omega^2 \tau_r^2}. \quad (2)$$
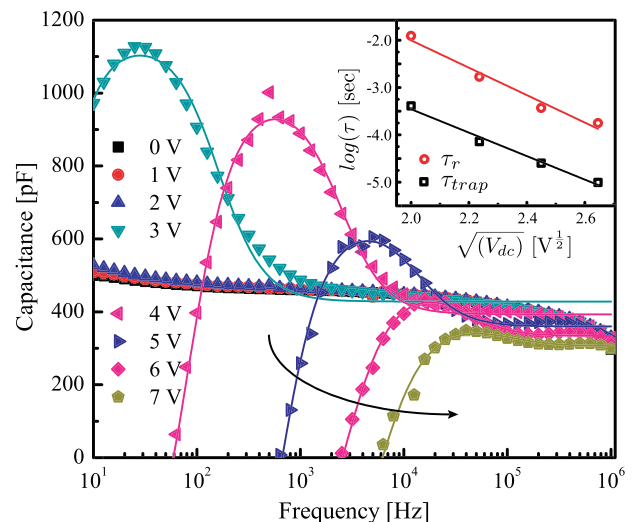

FIG. 1. Current-voltage-luminance and capacitance-voltage ($f = 100$ Hz) characteristics of a BSB-Cz-based OLED. The inset shows the structure of the device. Q_m, Q_{ac}^t, and Q_r are charges on electrodes, trapped space charges, and recombination charges, respectively. These charges dominate at different V_{dc} regions.

FIG. 2. Frequency dependent capacitance at various V_{dc} (0 ~ 7 V). The solid lines are the fitting results obtained using Eq. (2). The arrow represents the increasing direction of V_{dc}. The inset shows the voltage dependences of the characteristic times τ_{trap} and τ_r, which follow the Poole-Frenkel relationship.

Here, χ_1 and χ_2 are dimensionless constants. Although Eq. (2) is very simple, it still maintains the basic characteristics of frequency-dependent complex capacitance, i.e., the Cole-cole relation.[24] In addition, the equation readily describes the experimental results, which are shown as solid lines in Fig. 2. ==The obtained characteristic times and their voltage dependence are depicted in the inset of Fig. 2, which exhibited a Poole-Frenkel relation.[13–16,25]== The obtained trapping time (τ_{trap}) and recombination time (τ_r) correspond to the transit times of holes and electrons, respectively, which will be discussed further below.

The transit times for holes (τ_{tr}^h) and electrons (τ_{tr}^e) were obtained from the frequency-dependent susceptance of the OLED, which is depicted in Fig. 3. In Fig. 3, the sharp peaks at higher frequency are attributed to hole transitions, while, the broad low frequency peaks are ascribed to electron transport. The peak structures for electron transport are more obvious on log-log scale, as shown in the lower inset of Fig. 3. The transit times were obtained ($\tau_{tr} = 0.29\tau_{peak}$)[26] and their dependence on dc bias is shown in the upper inset of Fig. 3. It is found that both the transit times followed the Poole-Frenkel relationship, although the slopes were different. A stronger voltage dependence of the electron transit has also been reported for other materials, and was attributed to the electron trapping process.[15,27] In fact, the wide distribution of the electron mobility also implied a trapping modified electron transport process. Taking into consideration the differences in device structure, the mobility calculated from impedance spectroscopy ($\mu = L^2/\tau_{tr}V_{dc}$) corresponded well to that obtained from time-of-flight measurements.[21] The hole mobility obtained from impedance spectroscopy was about 7.29×10^{-5} cm^{2}V^{-1}s^{-1} at 3.7×10^5 V/cm, which was about one order lower than that estimated from the time-of-flight measurements about 7×10^{-4} cm^{2}V^{-1}s^{-1} at 2.5×10^4 V/cm. It is suggested that the different device structures used in those experiments should be responsible for the observed deviations. However, the voltage dependent mobility and higher value of hole mobility than electron mobility were well

revealed from both experiments. In addition, compared with other obtained characteristic times in Fig. 2, it is suggested that the hole transit time ($\tau_{tr}^h \approx 10^{-6} - 10^{-5}$ s) is the shortest, followed by the hole trapping time ($\tau_{trap} \approx 10^{-5} - 10^{-4}$ s). On the other hand, the electron transit time (τ_{tr}^e) is similar to the recombination time ($\tau_r \approx 10^{-4} - 10^{-2}$ s), implying the recombination process is limited by the electron current. All of the characteristic times exhibit the Poole-Frenkel relationship, which is important for understanding the capacitance-voltage relationship.

Figure 4 shows the capacitance-voltage relationships of the OLED at various frequencies. As ==V_{dc} increased, τ_{trap}, τ_r, and τ_{tr} decreased correspondingly, as shown in Fig==s. 2 and 3. Their relative values with respect to τ_{ac} determined the C–V characteristics of the OLED. At high frequency ($\tau_{ac} < \tau_{tr} < \tau_{trap} < \tau_r$), carriers are not able to respond to the ac signal, resulting in a voltage independent capacitance. As frequency decreased ($\tau_{tr} < \tau_{trap} < \tau_r < \tau_{ac}$), the redistribution of injected charges and recombination processes occurred. For different frequencies, the C–V characteristics varied gradually, suggesting a "mapping" or "frozen" process for the carriers with slower characteristic times, i.e., $\tau_{ac} < \tau_{trap} < \tau_r$. Here, because the recombination process undermined carrier density, we focused on the trapping processes with τ_{trap}.

The calculated ac characteristic time-dependent trapped carrier density is shown in the inset of Fig. 4. Firstly, at one V_{dc}, the amount of trapped space charges at one τ_{ac} interval was estimated to be around 10^{15} cm^{-3}, which seems reasonable. The total amount of trapped charge at one dc bias can be calculated by summation over the whole time range. In addition, the carrier density distribution is located within some τ_{ac} region. This is because, on one hand, fast carriers may travel across the device without trapping ($\tau_{tr} < \tau_{ac} < \tau_{trap}$), resulting in little contribution to capacitance.[28] On the other hand, slow carriers ($\tau_{trap} \sim \tau_r \sim \tau_{tr}^e < \tau_{ac}$) will recombine with injected electrons, leading to negative capacitance. In fact, the obtained trapped charge distributed between τ_{tr}^h and
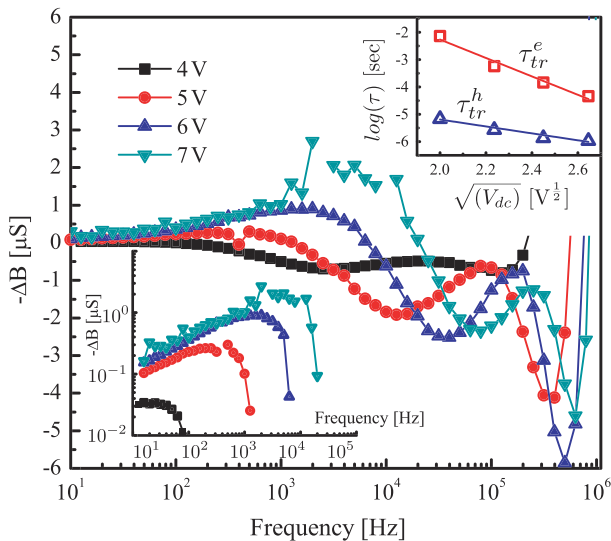

FIG. 3. Frequency dependence of susceptance ($-\Delta B = -\omega(C - C_g)$) at various voltages. The lower inset shows the susceptance on a log-log scale. The upper inset shows the voltage dependence of the obtained transit times of electrons (τ_{tr}^e) and holes (τ_{tr}^h).
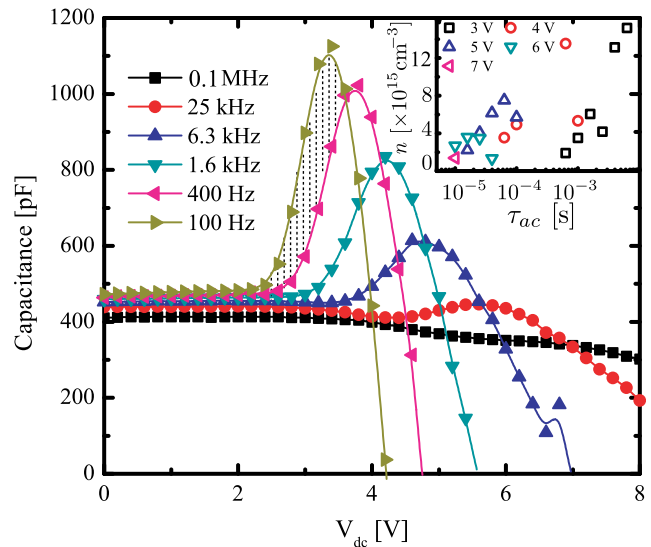

FIG. 4. Capacitance-voltage characteristics of the device at frequencies from 100 Hz to 0.1 MHz. The inset shows the calculated carrier density distribution with respect to ac characteristic time τ_{ac}. The shaded area shows the total trapped carrier amount distributed between 2.4 and 3.6 V in one τ_{ac} region from 10^{-2} to 2.5×10^{-3} s.

$\tau_{tr}^e (\sim \tau_r)$ corresponds well to the proposed model.[13,14] With the increase in V_{dc}, the characteristic times shortened, resulting in a shift of distribution to the shorter τ_{ac} regions as shown in the inset of Fig. 4.

In conclusion, the capacitance-voltage characteristics of a highly fluorescent BSB-Cz-based OLED were studied with a focus on the space charge distribution, and characteristic times and their distribution. The characteristic times and their bias dependences were obtained from the frequency dependence, which exhibited the Poole-Frenkel relationship. In addition, the time distributions of the trapped charges were revealed from the capacitance-voltage dependence at various frequencies. It is suggested that the voltage-dependent characteristic times and their distribution in time domains are responsible for the observed changes in capacitance. The conclusions are expected to be of help to further understand the carrier behaviour in low mobility systems, such as organic photovoltaic cells (OPVs), especially the bipolar carrier transport process and trapping effect.[29]

[1]S. R. Forrest, Nature **428**, 911 (2004).
[2]H. Uoyama, K. Goushi, K. Shizu, H. Monura, and C. Adachi, Nature **492**, 234 (2012).
[3]W. Brütting and C. Adachi, *Physics of Organic Semiconductors*, 2nd ed. (Wiley-VCH, Berlin, 2012).
[4]W. Brütting, S. Berleb, and A. G. Muckl, Org. Electron. **2**, 1 (2001).
[5]H. Bässler and A. Köhler, Top. Curr. Chem. **312**, 1 (2011).
[6]Y. Zhang and S. R. Forrest, Phys. Rev. Lett. **108**, 267404 (2012).
[7]A. Köhler and H. Bässler, Mater. Sci. Eng. R. **66**, 71 (2009).
[8]B. H. Wallikewitz, D. Kabra, S. Gelinas, and R. H. Friend, Phys. Rev. B **85**, 045209 (2012).
[9]L. Zhang, D. Taguchi, J. Li, T. Manaka, and M. Iwamoto, Appl. Phys. Lett. **98**, 092109 (2011).
[10]L. Zhang, D. Taguchi, H. Masada, T. Manaka, and M. Iwamoto, Jpn. J. Appl. Phys. Part 1 **51**, 02BK08 (2012).
[11]I. H. Campbell, D. L. Smith, and J. P. Ferraris, Appl. Phys. Lett. **66**, 3030 (1995).
[12]S. Nowy, W. Ren, A. Elschner, W. Lövenich, and W. Brütting, J. Appl. Phys. **107**, 054501 (2010).
[13]H. C. F. Martens, H. B. Brom, and P. W. M. Blom, Phys. Rev. B **60**, R8489 (1999).
[14]S. Berleb and W. Brütting, Phys. Rev. Lett. **89**, 286601 (2002).
[15]H. C. F. Martens, J. N. Huiberts, and P. W. M. Blom, Appl. Phys. Lett. **77**, 1852 (2000).
[16]D. Poplavskyy and F. So, J. Appl. Phys. **99**, 033707 (2006).
[17]S. Ishihara, H. Hase, T. Okachi, and H. Naito, J. Appl. Phys. **110**, 036104 (2011).
[18]H. C. F. Martens, W. F. Pasveer, H. B. Brom, J. N. Huiberts, and P. W. M. Blom, Phys. Rev. B **63**, 125328 (2001).
[19]E. Ehrenfreund, C. Lungenschmied, G. Debbler, H. Neugebauer, and N. S. Sariciftci, Appl. Phys. Lett. **91**, 012112 (2007).
[20]V. Shrotriya and Y. Yang, J. Appl. Phys. **97**, 054504 (2005).
[21]Y. Setoguchi and C. Adachi, J. Appl. Phys. **108**, 064516 (2010).
[22]M. A. Lampert and P. Mark, *Current Injection in Solids* (Academic Press, New York, 1970).
[23]J. M. Mentero, J. Bisquert, G. G. Belmonte, H. J. Bolink, and E. M. Barea, Phys. Status Solidi A **204**, 2402 (2007).
[24]K. C. Kao, *Dielectric Phenomena in Solids* (Elsevier Academic, San Diego, 2004).
[25]L. S. C. Pingree, B. J. Scott, M. T. Russell, T. J. Marks, and M. C. Hersam, Appl. Phys. Lett. **86**, 073509 (2005).
[26]M. Schmeits, J. Appl. Phys. **101**, 084508 (2007).
[27]P. W. M. Blom, M. J. M. de Jong, and J. J. M. Vleggaar, Appl. Phys. Lett. **68**, 3308 (1996).
[28]L. Zhang, D. Taguchi, T. Manaka, and M. Iwamoto, J. Appl. Phys. **110**, 033715 (2011).
[29]H. P. Gommans, M. Kemerink, and R. A. J. Janssen, Phys. Rev. B **72**, 235204 (2005).